Design and Fabrication of Grating Couplers for the Optical Addressing of Trapped Ions

Yu Dian Lim, Hong Yu Li, Peng Zhao, Jing Tao, Luca Guidoni, and Chuan Seng Tan, *Senior Member, IEEE*

***Abstract*—In this work, silicon photonics structures for the optical addressing of trapped ion is developed for quantum computing applications. Grating-waveguide-grating structures of various designs are designed, and fabricated for various radius curvatures of 12, 15, 25 and 30 μm, respectively. From the optical measurements, gratings with radius of curvature of 25 and 30 μm exhibit lower power loss of 36.5 and 33.9 dB with better-focused beam profiles as compared to those with radius of curvature of 12 and 15 μm. The beam width from these gratings ranges between 17.31 to 41.54 μm, which provides the feasibility to perform optical addressing on 2 to 4 Sr^+ ions trapped along the ground electrode of the ion trap.**

***Index Terms*—Silicon photonics, ion trap, ion qubits, quantum computing.**

I. Introduction

THE past decade has been exciting years for the development of quantum computing. In year 2016, International Business Machines Corporation (IBM) has introduced a quantum cloud service, IBM Q. Utilizing the 16-qubit and 20-qubit processors, the superconductor-based quantum computing device, IBM Q provides high fidelity quantum gate operations and measurements [1]. Meanwhile, Google Inc. claimed quantum supremacy by introducing Sycamore processor where the largest random quantum circuits have 53 qubits, 1113 single-qubit gates, and 430 two-qubit gates. With 0.2% fidelity, Sycamore processor is able to perform a complex computing task in 200s, of which a state-of-the-art classical supercomputer would take approximately 10000 years [2], [3].

Quantum computing uses the quantum phenomena of qubits (superposition and entanglement) to perform complex computing tasks [4]. Over the past decades, various qubit species have been realized, including superconducting qubits [2], [5], semiconductor quantum dots [6], [7], and trapped ion qubits [8]. Among the abovementioned qubits, trapped ion qubits received much attentions due to its high fidelity in quantum entanglement, as trapped ions are intrinsically identical [9]. To apply trapped ion qubits in quantum computing device, Honeywell implemented QCCD (quantum charge-coupled device) architecture into a programmable trapped ion quantum computer. In the QCCD, trapped ion quantum computer can be achieved by integrating ion trap with optoelectronic components for optical addressing of qubits, into a compact, standalone device. It has been reported that QCCD achieved a quantum volume measurement of 2^4 with negligible cross-talk [10].

As mentioned earlier, optoelectronic components are needed in trapped ion quantum computer for the optical addressing of ion qubits. By integrating optoelectronics, such as silicon photonic components into ion trap, the quantum computer can be realized on-chip, where the fabrication can be done using conventional CMOS fabrication technique on silicon-based platforms [4]. A pioneering work on the photonic integration of ion trap-based quantum computing device was reported by Mehta et al. In the reported work, silicon photonics circuit was integrated in the planar ion trap, utilizing optimized grating coupler design to "aim" the output laser beam towards trapped ion for quantum computing operation Fig. 1(b) [11], [12]. The integrated photonics have then been further expanded in the latter work, where optical addressing of trapped ion qubits have been realized using grating couplers of various designs, which corresponds to various laser wavelengths required for qubit operations [13].

In our previous works, we have developed a optical addressing technique that integrates silicon photonic components with planar electrode ion trap (Patent number: WO 2021/006811A) [14]. An opening is fabricated on the ground (GND) electrode to facilitate optical addressing, as shown in Fig. 1(a). Meanwhile, an ion trapping site can be formed on top of the GND surface electrode by simulating and optimizing combined direct current (DC)/radio frequency (RF) electric field (Fig. 2(a)) [15]. From the ion trapping experiment, 3 Sr^+ ions are trapped at the ion-trapped site [16]. As mentioned earlier, focused, integrated photonic components are required for the optical addressing trapped ion in realizing its quantum computing applications.

Manuscript received May 31, 2021; revised June 28, 2021; accepted June 30, 2021. Date of publication July 7, 2021; date of current version August 2, 2021. This work was supported in part by the A*STAR Quantum Technology for Engineering program (A1685b0005), in part by the National Research Foundation, Singapore under its ANR-NRF Joint Grant Call (NRF2020-NRF-ANR073 HIT), and in part by the A∗STAR Institute of Microelectronics (IME) and Advanced Micro Foundry (AMF). *(Corresponding authors: Yu Dian Lim and Chuan Seng Tan.)*

Yu Dian Lim, Jing Tao, and Chuan Seng Tan are with the School of Electrical and Electronics Engineering, Nanyang Technological University, Singapore 639798, Singapore (e-mail: yudian.lim@ntu.edu.sg; taojing@ntu.edu.sg; tancs@ntu.edu.sg).

Hong Yu Li is with the Institute of Microelectronics, Agency for Science, Technology and Research (A∗STAR), Singapore 117685, Singapore (e-mail: lihy@ime.a-star.edu.sg).

Peng Zhao is with the School of Electrical and Electronics Engineering, Nanyang Technological University, Singapore 639798, Singapore, and also with the Institute of Microelectronics, Agency for Science, Technology and Research (A∗STAR), Singapore 117685, Singapore (e-mail: zhao0275@e.ntu.edu.sg).

Luca Guidoni is with the Laboratoire Matériaux et Phénomènes Quantiques (MPQ), Université de Paris, F-75205 Paris, France (e-mail: luca.guidoni@univ-paris-diderot.fr).

This article has supplementary downloadable material available at http://10.1109/JPHOT.2021.3094646, provided by the authors.

Digital Object Identifier 10.1109/JPHOT.2021.3094646

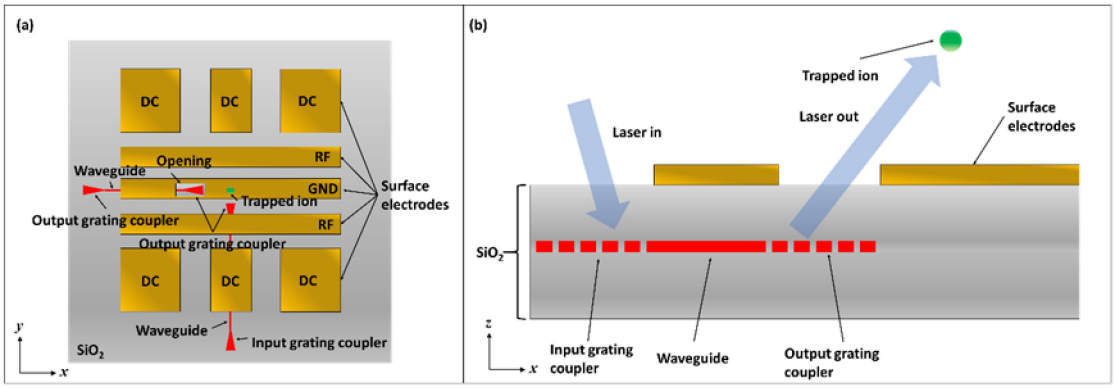

Fig. 1. (a) Top view, (b) Side view of photonics integrated planar ion trap.

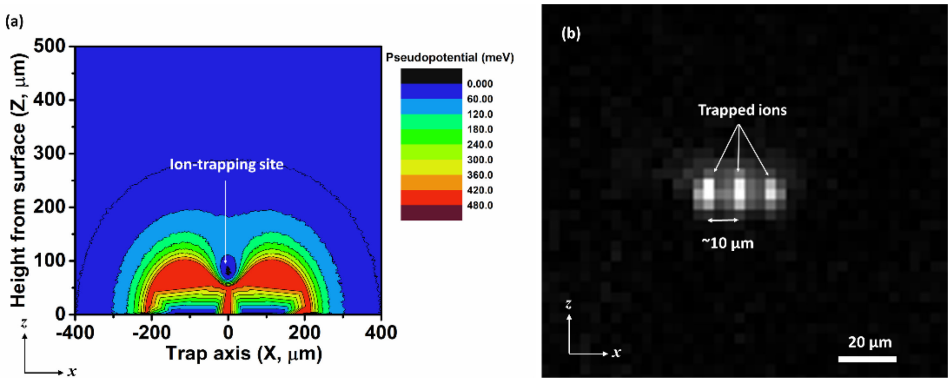

Fig. 2. (a) Pseudopotential distribution at xz-plane, (b) Image of trapped strontium ions under CCD camera.

However, there has been limited work on the investigation, design and optimization of grating couplers for optical addressing application.

In this study, grating couplers of various designs are fabricated and optimized. The pitch size and duty cycle of the grating is fixed; while the radius of curvatures varies. The coupling efficiency of various grating couplers are then measured and investigated. Meanwhile, the beam profile of the laser beam coupled out from the grating coupler is also acquired and analyzed. The obtained results from this study give preliminary understanding on the beam profiling and focusing of grating coupler with various radius of curvatures, which provide insightful information when designing grating coupler for optical addressing applications.

II. Experimental Details

The fabrication of silicon photonics passive components is carried out on 200 mm Silicon-On-Insulator (SOI) wafer with 220 nm Silicon (Si) device layer and 2 μm buried oxide (BOX) layer. The dimension of Si strip waveguide is fixed at 500 nm width and 220 nm height; whereas the grating designs are fixed at 110 nm etch depth, 0.63 duty cycle and 650 nm pitch size. The length of the waveguides between the input and output grating couplers is fixed at 1000 μm. The details of the fabrication process are illustrated in Supplementary Fig. 1. The measurements and beam profiling are carried out on grating-waveguide-grating test structures, as illustrated in Fig. 3(b). The labeling of the investigated samples is illustrated in Fig. 4.

Fig. 3(a) and (b) show the beam profiling system setup and the schematic diagram of the test structure, respectively. Prior to the beam profiling, the coupling efficiency of the grating-waveguide-grating test structures is measured. The coupling efficiency is measured by coupling laser beam (10 dBm, 1630 nm) into the input grating coupler via input fiber, the laser beam coupled from the output grating coupler to the output fiber for power measurement. A 3-panel polarizer is used to optimize polarization of the laser light.

The beam profiling is carried out using Xeva XC-130 Beam Profiling Camera with Navitar $\times 6.5$ camera with $\times 2$ optical adapter. Prior to beam profiling, the input and output fibers are coupled to input and output grating couplers, respectively, to obtain optimized power output from the output grating coupler at 1630 nm wavelength, where the optimized power was reflected from the power meter (Fig. 3(a)). After obtaining the optimized power output, the output fiber is shifted to avoid obstructing the light from the output grating coupler, and the beam profiling camera is then positioned to obtain the beam. The beam from the output grating coupler is then focused towards the beam profiling camera using objective lens. The obtained beam profiling is recorded and analyzed using BeamGage software.

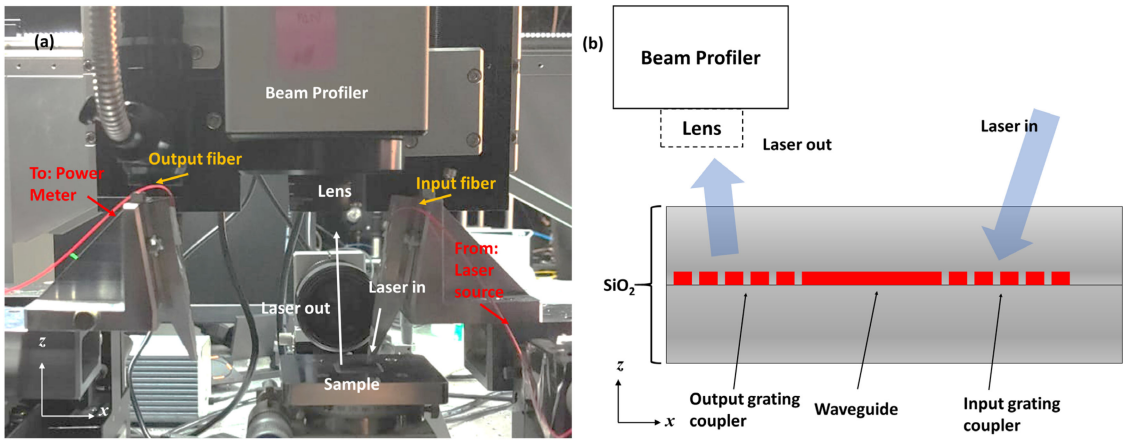

Fig. 3. Optical power measurement and beam profiling system setup: (a) Photograph, (b) Schematic diagram.

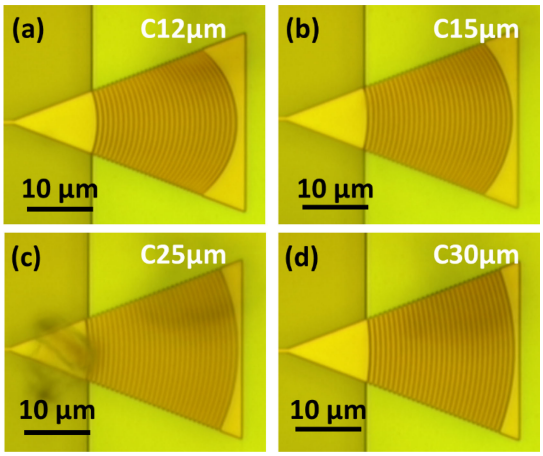

Fig. 4. Labelling of the grating coupler design: (a) C12 µm, (b) C15 µm, (c) C25 µm, (d) C30 µm.

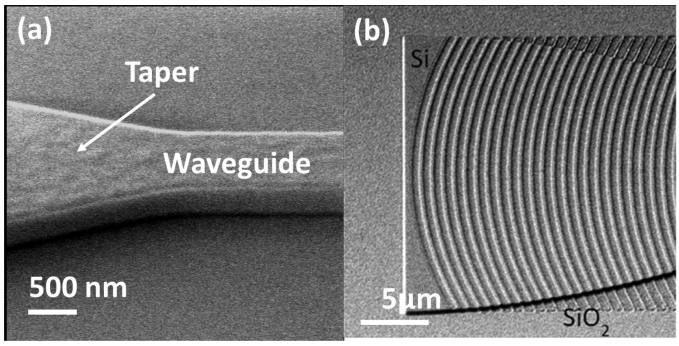

Fig. 5. SEM images of: (a) taper and waveguide, (b) grating structure.

III. Results and Discussion

Fig. 5(a) shows the typical Scanning Electron Microscope (SEM) image of taper-waveguide joint with the taper fabricated with the grating coupler. In a typical measurement process, laser light will propagate from the grating coupler to waveguide (or vice versa). At the same time, Fig. 5(b) shows the SEM image of the grating structure, where ordered, periodical structure was achieved for the coupling of laser light into/from the grating.

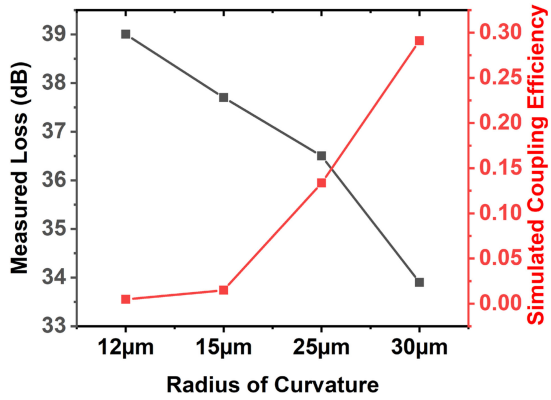

Fig. 6. Optical power loss from grating-waveguide-grating test structure.

Fig. 6 shows the optical power simulation and measurement of grating coupler with various radius of curvature. From the simulation, it is shown that the coupling efficiency increases with increasing radius of curvature. The coupling efficiencies of C12 µm and C15 µm are relatively low (0.5 – 1.5%) as compared to C25 µm and C30 µm (13 and 29%). On the other hand, power loss of 39, 37.7, 36.5, and 33.9 dB has been obtained for C12 µm, C15 µm, C25 µm, and C30 µm, respectively. The simulated results align well with the measurement results where the power loss reduces as the radius of curvature increases. Nevertheless, discrepancies between simulation-measurement results are anticipated where external factors such as manufacturing errors and non-optimized fiber-to-grating alignment. Based on our previous studies, the propagation loss of the waveguide is estimated to be ~1.15 dB/cm [17], [18]. When both input and output grating coupler has similar coupling efficiencies with negligible waveguide propagation loss, the coupling losses of each C12 µm, C15 µm, C25 µm, and C30 µm grating coupler can be deduced as 19.5, 18.85, 18.25, 16.95 dB, respectively.

The power losses obtained from C12 μm, C15 μm, C25 μm, and C30 μm grating couplers range between 16.95 to 19.5 dB. These power losses are relatively higher as compared to the state-of-the-art grating couplers fabricated on silicon-on-insulator (SOI) platforms [19]–[22]. Fundamentally, the power losses and coupling efficiency of grating couplers rely on the grating's design, including silicon (Si) device layer thickness, etch depth, duty cycle, pitch and the fiber-to-grating alignment angle. As the fabrication is carried out on standard 220 nm Si layer SOI wafer, the Si device layer is fixed. To explore possible influence of the etch depth, duty cycle, and pitch on the grating coupler performance, first, the simulated coupling efficiency at Si etch depth between 10 to 220 nm is explored (Supplementary Fig. 2). Note that simulation results presented in Supplementary Fig. 2 were obtained from two-dimensional simulation condition, which considers only the etch depth, duty cycle, fiber-to-grating angle and pitch size without considering the three-dimensional factors such as taper shape, taper size, and radius of curvature; whereas simulated coupling efficiencies in Fig. 6 were obtained from three-dimensional simulation condition with three-dimensional factors taken under consideration. Up to 180 nm, the 110 nm etch depth employed in this study has the optimal coupling efficiency. Although 220 nm etch-through may yield higher coupling efficiency, however, etching-through Si device layer may cause back-scattering of etchant, especially in fabricating grating structure. This will result in high sidewall roughness, which will susceptibly cause higher coupling loss [23]–[25]. Nevertheless, as the gratings are fabricated under multi-project wafer (MPW), the etch depth is fixed. Thus, the 110 nm etch depth employed in this study shall be fixed.

Other possible factors influencing the coupling efficiency of gratings include pitch size and duty cycle. To explore the variations of duty cycle and pitch size on the coupling efficiencies, the coupling efficiencies at various duty cycle and pitch sizes are simulated (Supplementary Fig. 3). Note that the 650 nm pitch size and 0.63 duty cycle are not the most ideal combination in terms of input coupling efficiencies. For instance, it is possible that the coupling efficiency can be doubled when the pitch size increases to 810 nm. However, the 650 nm pitch size and 0.63 duty cycle in this study are employed based on the direction of which the 1630 nm light coupled out from the grating coupler. In designing the grating couplers used in this study, the pitch size and the duty cycle are designed such that the output light coupled out from the grating will be propagated vertically upwards, reaching the beam profiler located on top of the sample as shown in Fig. 3. This also aligns with the design of photonics-integrated ion trap reported in our earlier technology disclosure, where grating couplers can be located right below the trapped ions for optical addressing. The simulated propagation of the 1630 nm coupled out from gratings with 650 nm pitch size and 0.63 duty cycle is shown in Supplementary Fig. 4.

Besides the abovementioned factors, other factors such as sidewall roughness of the grating structures, and fiber-to-grating alignment can also influence the coupling efficiency of gratings. For instance, high sidewall roughness in the grating will cause severe scattering when light is coupled into the grating, as aligned with the previously-reported studies [26], [27]. At the same time, the fiber is aligned $\sim 10^{\circ}$ to the normal of the grating coupler. It is also possible that the angle of alignment can be tuned to obtain higher coupling efficiency and lower coupling loss [19], [20]. However, due to the limitations in equipment and resources, further investigations in these directions are challenging at this stage of the research. For instance, as the grating couplers investigated in this work is fabricated through MPW, the optimization of sidewall roughness is not feasible at our side. Nevertheless, the main objective of this work is to develop grating couplers for the optical addressing of trapped ions. The estimated intensities required for this application can range widely between $10 - 100000\,\mathrm{mW/cm^2}$ [28]. In this context, both coupling efficiencies and the beam profiles coupled out from gratings with various designs, radius of curvatures shall be equally considered. Thus, the future work derived from this study can utilize the preliminary coupling efficiencies and beam profiles obtained from this work to further optimize the coupling performance, such as optimizing the fiber-to-grating alignment, minimizing the sidewall roughness, etc.

For optimal coupling of light into the waveguide through grating coupler, phase match condition shall be fulfilled under the following condition:

$$\Lambda = \frac{\lambda}{N - n_1 \sin\theta} \tag{1}$$

where Λ is the grating pitch, λ is the wavelength of the light, N is the effective index, $\mathrm{n_1}$ is the refractive index of the SiO_2 cladding, and θ is the inclination angle between input fiber and the input grating coupler [29]. The coupling efficiency of the grating coupler can be expressed as:

$$\eta = \left| E\left(x, z = z_0\right) A e^{\frac{-(x-x_0)^2}{w_0^2}} e^{jy\frac{2\pi}{\lambda} n_1 \sin\theta} dy \right|^2 \tag{2}$$

where A is a constant describing the laser beam characteristics, w_0 is the beam width coupled to grating coupler, and x is the distance parallel to the waveguide axis, z is the separation between the input fibre and the top of the input grating, which is fixed at z_0 [30]. Despite expressing the coupling efficiency of grating coupler, (2) does not include characteristics of the grating coupler such as pitch, duty cycle, etch depth, etc [31]. Part of the characteristics were included in (1), such as the grating pitch, Λ. Both (1) and (2) do not include radius of curvature and other external factors of grating coupler. Nevertheless, it is possible that these factors (e.g., radius of curvature) are affecting $E(x, z)$ term, which in turn affect the coupling efficiency and coupling loss.

Apart from the coupling loss, another important factor in optical addressing is the beam width of the light coupled out from the grating. Fig. 7 shows the beam profile obtained from the fabricating grating couplers under the same height. Overall, the laser beams coupled out from the gratings are located at similar height, regardless of their respective radius of curvatures. This agrees well with the simulated beam profile presented in Supplementary Fig. 2 where the beams obtained are located at the same spot, regardless of their radius of curvature. As the inclination direction of the output beams are affected by

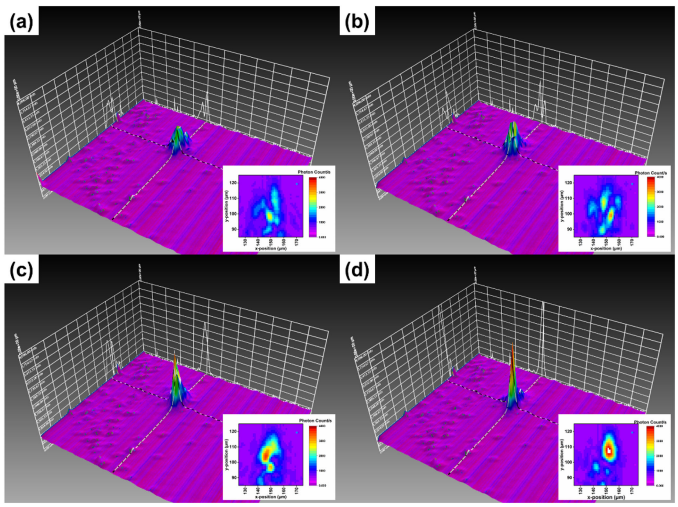

Fig. 7. Measured beam profiles coupled from (a) C12 μm, (b) C15 μm, (c) C25 μm, and (d) C30 μm grating couplers.

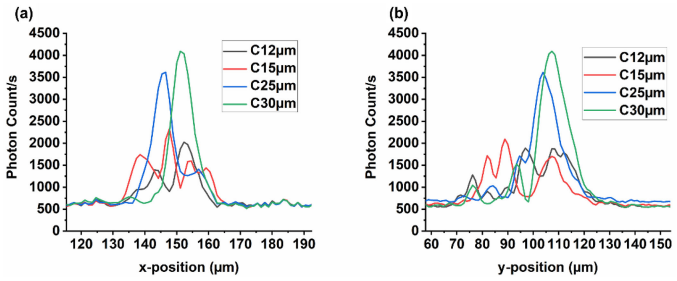

Fig. 8. Intensity distribution (count/s) of C12 μm, C15 μm, C25 μm, and C30 μm gratings along (a) x-axis, (b) y-axis.

other factors such as duty cycle, etch depth, and pitch size of the gratings, it can be deduced that the radius of curvature has minimal effects on the inclination direction of the output beams. From the beam profiles, it can be observed that C25 μm and C30 μm grating couplers exhibit more focused beam profile as compared to C12 μm and C15 μm, similar to the simulated beam profiles presented in Supplementary Fig. 2. This agrees well with the measured loss presented in Fig. 6 where the coupling losses of C12 μm and C15 μm grating couplers are higher than their C25 μm and C30 μm counterparts. At the same time, the photon count distribution and beam shape of the C25 μm and C30 μm grating couplers are similar to the simulated beams (Supplementary Fig. 3) with slightly larger beam sizes. This can be attributed to the non-ideal focusing of the beam during the profiling. The widths of the laser beams coupled from the gratings along x- and y-directions are shown in Fig. 8.

Fig. 8 shows the intensity distribution of the beam along x- and y-directions. From Fig. 8(a), C25 μm and C30 μm show sharp peaks with high photon counts along x-direction, whereas C12 μm and C15 μm gratings exhibit multiple low intensity peaks due to inferior focusing. Similar phenomenon is observed in Fig. 8(b) where C25 μm and C30 μm show sharper, higher intensity peaks as compared to their C12 μm and C15 μm counterparts. Intuitively, the sharp peaks and focused beam obtained by C25 μm and C30 μm gratings can partially explain the lower coupling loss (as compared to C12 μm and C15 μm) obtained, as presented in Fig. 6. Thus, C25 μm and C30 μm can be utilized for the optical addressing of trapped ion qubits for quantum computing applications, as illustrated in Fig. 1.

It has been observed that the beam waists along x-axis and y-axis are different. This phenomenon is observed in both experimental measurement (Fig. 7) and simulation (Supplementary Fig. 5). Generally, the beams exhibit oval shapes with the beam waist along y-axis larger than the beam waist along x-axis. Theoretically, the focusing along the direction of waveguide propagation (x-axis as referred to Fig. 7 and Supplementary Fig. 5) is determined by the grating pitch, duty cycle, and grating length. On the other hand, the focusing along y-axis is controlled by the radius of curvature [32]. In principle, varying the radius of curvature should have minimal influence on the beam waist along x-axis. However, changes in beam waist along x-axis are observed across radius of curvature from 12 to 30 μm. This can be attributed to the variation in coupling loss experienced by C12 μm, C15 μm, C25 μm and C30 μm grating couplers, as presented in Fig. 6. Nevertheless, the obtained beam profile provides preliminary insights on the feasibilities of the fabricated grating coupler in performing optical addressing of trapped ion qubits.

To realize the optical addressing of ion qubits, the placement of the grating coupler and the separation distance between adjacent ions are crucial. As referred to the CCD image of trapped ions (Fig. 2b), the separation distance between ions is approximately 10 μm. Meanwhile, the grating-waveguide-grating structure can be placed along x- or y-axis as illustrated in Fig. 1(a). From Fig. 8(a), the beam widths from C25 μm and C30 μm along x-axis are 24.23 and 17.31 μm, respectively. As the ions are trapped along GND electrode (ref. Fig. 1(a)), the beam width along x-axis corresponds to the placement of the grating-waveguide-grating structure along x-axis. In this context, the grating-waveguide-grating structure can be placed either along x- or y-axis, depending on the numbers of trapped ions to be optically addressed. It is possible for C25 μm grating to simultaneously perform optical addressing on 3 ions; whereas C30 μm grating is able to perform optical addressing on 2 ions simultaneously. On the other hand, the beam widths from C25 μm and C30 μm along y-axis are 41.54 and 35.77 μm, respectively. This corresponds to performing optical addressing of ∼4 ions trapped along GND electrode. Nevertheless, the number of ions of which respective grating couplers can reach can be varied, as the inter-ion distances can be fine-tuned (+/−3 μm) by DC voltages. Despite so, the obtained beam profiles provide preliminary insights on their feasibilities in performing optical addressing on ions and the number of ions where each grating designs can reach [33].

IV. Conclusion

In this work, grating-waveguide-grating structures for the optical addressing of trapped ion have been developed and characterized. The on-chip planar electrode ion trap design is based on the 5-wire Paul trap design, where the grating-waveguide-grating structure can be placed along x- or y-axis beneath the

electrodes. Grating couplers with radius of curvatures 12 to 30 μm are fabricated and labelled as C12 μm, C15 μm, C25 μm and C30 μm, and their respective feasibility in performing optical addressing on trapped ion qubits is evaluated. From the optical measurements, C25 μm and C30 μm gratings exhibit lower power loss of 36.5 and 33.9 dB with better-focused beam profiles as compared to C12 μm and C15 μm. The beam widths from these gratings range between 17.31 to 41.54 μm, which is feasible for performing optical addressing on 2 to 4 ions trapped along the ground electrode of the ion trap. The obtained results from this study provide preliminary insights on the integration of photonics components into planar electrode ion trap. This further eases the photonics integration of planar electrode ion trap for its application in scalable quantum computing devices.

REFERENCES

[1] Y. Wang, Y. Li, Z. qi Yin, and B. Zeng, "16-qubit IBM universal quantum computer can be fully entangled," *NPJ Quantum Inf.,* vol. 4, no. 1, pp. 1–6, 2018, doi: 10.1038/s41534-018-0095-x.

[2] F. Arute *et al.*, "Quantum supremacy using a programmable superconducting processor," *Nature*, vol. 574, no. 7779, pp. 505–510, 2019, doi: 10.1038/s41586-019-1666-5.

[3] S. Boixo *et al.*, "Characterizing quantum supremacy in near-term devices," *Nat. Phys.*, vol. 14, no. 6, pp. 595–600, 2018, doi: 10.1038/s41567-018-0124-x.

[4] C. D. Bruzewicz, J. Chiaverini, R. McConnell, and J. M. Sage, "Trapped-ion quantum computing: Progress and challenges," *Appl. Phys. Rev.*, vol. 6, no. 2, pp. 021314, 2019, doi: 10.1063/1.5088164.

[5] E. P. Debenedictis, "A role for IEEE in quantum computing," *Computer*, vol. 51, no. 8, pp. 52–55, 2018, doi: 10.1109/MC.2018.3191257.

[6] S. D. Liles *et al.*, "Spin and orbital structure of the first six holes in a silicon metal-oxide-semiconductor quantum dot," *Nat. Commun.*, vol. 9, no. 1, pp. 1–7, 2018, doi: 10.1038/s41467-018-05700-9.

[7] M. Veldhorst *et al.*, "A two-qubit logic gate in silicon," *Nature*, vol. 526, no. 7573, pp. 410–414, 2015, doi: 10.1038/nature15263.

[8] K. R. Brown, J. Kim, and C. Monroe, "Co-designing a scalable quantum computer with trapped atomic ions," *NPJ Quantum Inf.,* vol. 2, no. 1, pp. 1–10, 2016, doi: 10.1038/npjqi.2016.34.

[9] D.-I. "Dan" Cho, S. Hong, M. Lee, and T. Kim, "A review of silicon microfabricated ion traps for quantum information processing," *Micro Nano Syst. Lett.*, vol. 3, no. 1, p. 2, 2015, doi: 10.1186/s40486-015-0013-3.

[10] J. M. Pino *et al.*, "Demonstration of the trapped-ion quantum CCD computer architecture," *Nature*, vol. 592, pp. 209–213, 2021.

[11] K. K. Mehta, C. D. Bruzewicz, R. Mcconnell, R. J. Ram, J. M. Sage, and J. Chiaverini, "Integrated optical addressing of an ion qubit," *Nat. Nanotechnol.*, vol. 11, no. 12, pp. 1066–1070, 2016, doi: 10.1038/nnano.2016.139.

[12] K. K. Mehta, C. Zhang, M. Malinowski, T. L. Nguyen, M. Stadler, and J. P. Home, "Integrated optical multi-ion quantum logic," *Nature*, vol. 586, no. 7830, pp. 533–537, 2020, doi: 10.1038/s41586-020-2823-6.

[13] R. J. Niffenegger *et al.*, "Integrated multi-wavelength control of an ion qubit," *Nature*, vol. 586, no. 7830, pp. 538–542, 2020, doi: 10.1038/s41586-020-2811-x.

[14] Y. D. Lim, A. A. A. Apriyana, J. Tao, and C. S. Tan, "Device for trapping ion, method for forming the same, and method for controlling the same," PCT Patent Application Publication WO/2021/006811, Jan. 2021.

[15] J. Tao, H. Y. Li, P. Zhao, Y. D. Lim, A. A. A. Apriyana, and C. S. Tan, "Design considerations and fabrication challenges of surface electrode ion trap with TSV integration," in *Proc. IEEE 2019 Int. 3D Syst. Integr. Conf.*, pp. 7–11, 2019, doi: 10.1109/3DIC48104.2019.9058780.

[16] J. Tao *et al.*, "Large-scale fabrication of surface ion traps on a 300 mm glass wafer," *Phys. Status Solidi*, vol. 258, no. 7, p. 2000589, 2021, doi: 10.1002/pssb.202000589.

[17] Y. D. Lim *et al.*, "EO integration of planar ion trap and silicon photonics for optical addressing in quantum computing," in *Proc. Conf. Lasers Electro-Opt. (CLEO)*, San Jose, CA, USA, May 2020.

[18] Y. D. Lim, J. Tao, P. Zhao, A. A. A. Apriyana, and C. S. Tan, "Development and integration of silicon photonics interposer for quantum computing system," *IEEE Int. Conf. Gr. IV Photon. GFP*, vol. 2019, pp. 1–2, Aug. 2019, doi: 10.1109/GROUP4.2019.8853904.

[19] H. Y. Chen, S. Y. Xu, and K. C. Yang, "Design of a highly efficient uniform grating coupler with gradually etched grooves for silicon-on-insulator waveguides," in *Proc. Symp. Photon. Optoelectron*, 2012, pp. 1–4, doi: 10.1109/SOPO.2012.6271056.

[20] T. Sharma *et al.*, "Coupling performance enhancement using SOI grating coupler design," *Opt. Commun.*, vol. 427, pp. 452–456, Jul. 2018, doi: 10.1016/j.optcom.2018.06.012.

[21] G. Roelkens, D. Van Thourhout, and R. Baets, "High efficiency Silicon-on-Insulator grating coupler based on a poly-Silicon overlay," *Opt. Exp.*, vol. 14, no. 24, p. 11622, 2006, doi: 10.1364/OE.14.011622.

[22] R. Halir *et al.*, "Single etch grating couplers for mass fabrication with DUV lithography," *Opt. Quantum Electron.*, vol. 44, no. 12–13, pp. 521–526, 2012, doi: 10.1007/s11082-012-9563-2.

[23] H. Saghaei, P. Elyasi, and R. Karimzadeh, "Design, fabrication, and characterization of Mach–Zehnder interferometers," *Photon. Nanostructures - Fundam. Appl.*, vol. 37, no. Aug., Aug. 2019, Art. no. 100733, doi: 10.1016/j.photonics.2019.100733.

[24] C. Alonso-Ramos *et al.*, "Single-etch grating coupler for micrometric silicon rib waveguides.," *Opt. Lett.*, vol. 36, no. 14, pp. 2647–2649, 2011, doi: 10.1364/OL.36.002647.

[25] G. T. Reed and A. P. Knights, *Silicon Photonics: An Introduction*. West Sussex, U.K.: Wiley, 2004.

[26] F. Grillot, L. Vivien, S. Laval, D. Pascal, and E. Cassan, "Size influence on the propagation loss induced by sidewall roughness in ultrasmall SOI waveguides," *IEEE Photon. Technol. Lett.*, vol. 16, no. 7, pp. 1661–1663, Jul. 2004, doi: 10.1109/LPT.2004.828497.

[27] C. Qiu *et al.*, "Fabrication, characterization and loss analysis of silicon nanowaveguides," *J. Lightw. Technol.*, vol. 32, no. 13, pp. 2303–2307, 2014, doi: 10.1109/JLT.2014.2309122.

[28] K. K. Mehta, "Integrated optical quantum manipulation and measurement of trapped ions," Ph.D. dissertation, Dept. Elect. Eng. Comput. Sci., Massachusetts Inst. Technol., Cambridge, MA, USA, 2017.

[29] M. J. Deen and P. K. Basu, "Guided lightwaves: Introduction," *Silicon Photon. I*, vol. 10, no. 8, 2012, pp. 265–301.

[30] L. Cheng, S. Mao, Z. Li, Y. Han, and H. Y. Fu, "Grating couplers on silicon photonics: Design principles, emerging trends and practical issues," *Micromachines*, vol. 11, no. 7, 2020, doi: 10.3390/mi11070666.

[31] J. C. Wirth, "Silicon grating couplers for low loss coupling between optical fiber and silicon nanowires," M.S. thesis, Dept. Elect. Comput. Eng., Purdue Univ., West Layette, IN, USA, 2011.

[32] K. K. Mehta, R. J. Ram, "Precise and diffraction-limited waveguide-to-free-space focusing gratings," *Sci. Rep.*, vol. 7, no. 1, pp. 1–8, 2017, doi: 10.1038/s41598-017-02169-2.

[33] M. Palmero, S. Martínez-Garaot, U. G. Poschinger, A. Ruschhaupt, and J. G. Muga, "Fast separation of two trapped ions," *New J. Phys.*, vol. 17, no. 9, pp. 4–13, 2015, doi: 10.1088/1367-2630/17/9/093031.